Study of the four-fermion final state at the Z resonance

D. Buskulic, D. Casper, I. de Bonis, D. Decamp, P. Ghez, C. Goy, J.P. Lees, M.N. Minard, P. Odier, B. Pietrzyk, et al.

CERN PPE/94-169
27 October 1994

Study of the four-fermion final state at the Z resonance

The ALEPH Collaboration*)

Abstract

The process $e^+e^- \to l\bar{l}f\bar{f}$, where l is a charged or a neutral lepton and f any charged fermion, is analyzed. The study uses the ALEPH data collected at LEP from 1989 to 1993 at centre-of-mass energies between 88 and 95 GeV, corresponding to almost two million hadronic Z decays and to a total integrated luminosity of 79 pb^{-1}. For all channels, the data agree well with the standard model expectation both in shape and normalization. The indication of an excess in the $e^+e^- \to \tau^+\tau^-f\bar{f}$ channel, reported by ALEPH in 1991, is not confirmed.

(Submitted to Zeitschrift für Physik)

---

*) See next pages for the list of authors

The ALEPH Collaboration

D. Buskulic, D. Casper, I. De Bonis, D. Decamp, P. Ghez, C. Goy, J.-P. Lees, M.-N. Minard, P. Odier, B. Pietrzyk

Laboratoire de Physique des Particules (LAPP), IN^{2}P^3-CNRS, 74019 Annecy-le-Vieux Cedex, France

F. Ariztizabal, M. Chmeissani, J.M. Crespo, I. Efthymiopoulos, E. Fernandez, M. Fernandez-Bosman, V. Gaitan, Ll. Garrido,[15] M. Martinez, S. Orteu, A. Pacheco, C. Padilla, F. Palla, A. Pascual, J.A. Perlas, F. Sanchez, F. Teubert

Institut de Fisica d'Altes Energies, Universitat Autonoma de Barcelona, 08193 Bellaterra (Barcelona), Spain[7]

D. Creanza, M. de Palma, A. Farilla, G. Iaselli, G. Maggi, N. Marinelli, S. Natali, S. Nuzzo, A. Ranieri, G. Raso, F. Romano, F. Ruggieri, G. Selvaggi, L. Silvestris, P. Tempesta, G. Zito

Dipartimento di Fisica, INFN Sezione di Bari, 70126 Bari, Italy

X. Huang, J. Lin, Q. Ouyang, T. Wang, Y. Xie, R. Xu, R. Xue, J. Zhang, L. Zhang, W. Zhao

Institute of High-Energy Physics, Academia Sinica, Beijing, The People's Republic of China[8]

G. Bonvicini, J. Boudreau,[25] P. Comas, P. Coyle, H. Drevermann, A. Engelhardt, R.W. Forty, M. Frank, G. Ganis, C. Gay,[3] M. Girone, R. Hagelberg, J. Harvey, R. Jacobsen, B. Jost, J. Knobloch, I. Lehraus, M. Maggi, C. Markou, E.B. Martin, P. Mato, H. Meinhard, A. Minten, R. Miquel, P. Palazzi, J.R. Pater, P. Perrodo, J.-F. Pusztaszeri, F. Ranjard, L. Rolandi, D. Schlatter, M. Schmelling, W. Tejessy, I.R. Tomalin, R. Veenhof, A. Venturi, H. Wachsmuth, W. Wiedenmann, W. Witzeling, J. Wotschack

European Laboratory for Particle Physics (CERN), 1211 Geneva 23, Switzerland

Z. Ajaltouni, M. Bardadin-Otwinowska, A. Barres, C. Boyer, A. Falvard, P. Gay, C. Guicheney, P. Henrard, J. Jousset, B. Michel, S. Monteil, J-C. Montret, D. Pallin, P. Perret, F. Podlyski, J. Proriol, J.-M. Rossignol, F. Saadi

Laboratoire de Physique Corpusculaire, Université Blaise Pascal, IN^{2}P^3-CNRS, Clermont-Ferrand, 63177 Aubière, France

T. Fearnley, J.B. Hansen, J.D. Hansen, J.R. Hansen, P.H. Hansen, S.D. Johnson, R. Møllerud, B.S. Nilsson

Niels Bohr Institute, 2100 Copenhagen, Denmark[9]

A. Kyriakis, E. Simopoulou, I. Siotis, A. Vayaki, K. Zachariadou

Nuclear Research Center Demokritos (NRCD), Athens, Greece

A. Blondel, G. Bonneaud, J.C. Brient, P. Bourdon, L. Passalacqua, A. Rougé, M. Rumpf, R. Tanaka, A. Valassi, M. Verderi, H. Videau

Laboratoire de Physique Nucléaire et des Hautes Energies, Ecole Polytechnique, IN^{2}P^3-CNRS, 91128 Palaiseau Cedex, France

D.J. Candlin, M.I. Parsons, E. Veitch

Department of Physics, University of Edinburgh, Edinburgh EH9 3JZ, United Kingdom[10]

E. Focardi, G. Parrini

Dipartimento di Fisica, Università di Firenze, INFN Sezione di Firenze, 50125 Firenze, Italy

M. Corden, M. Delfino,[12] C. Georgiopoulos, D.E. Jaffe

Supercomputer Computations Research Institute, Florida State University, Tallahassee, FL 32306-4052, USA [13,14]

A. Antonelli, G. Bencivenni, G. Bologna,[4] F. Bossi, P. Campana, G. Capon, F. Cerutti, V. Chiarella, G. Felici, P. Laurelli, G. Mannocchi,[5] F. Murtas, G.P. Murtas, M. Pepe-Altarelli, S. Salomone

Laboratori Nazionali dell'INFN (LNF-INFN), 00044 Frascati, Italy

P. Colrain, I. ten Have,[6] I.G. Knowles, J.G. Lynch, W. Maitland, W.T. Morton, C. Raine, P. Reeves, J.M. Scarr, K. Smith, M.G. Smith, A.S. Thompson, S. Thorn, R.M. Turnbull

Department of Physics and Astronomy, University of Glasgow, Glasgow G12 8QQ,United Kingdom[10]

U. Becker, O. Braun, C. Geweniger, P. Hanke, V. Hepp, E.E. Kluge, A. Putzer,[21] B. Rensch, M. Schmidt, H. Stenzel, K. Tittel, M. Wunsch

Institut für Hochenergiephysik, Universität Heidelberg, 69120 Heidelberg, Fed. Rep. of Germany[16]

R. Beuselinck, D.M. Binnie, W. Cameron, M. Cattaneo, D.J. Colling, P.J. Dornan, J.F. Hassard, N. Konstantinidis, L. Moneta, A. Moutoussi, J. Nash, D.G. Payne, G. San Martin, J.K. Sedgbeer, A.G. Wright

Department of Physics, Imperial College, London SW7 2BZ, United Kingdom[10]

G. Dissertori, P. Girtler, E. Kneringer, D. Kuhn, G. Rudolph

Institut für Experimentalphysik, Universität Innsbruck, 6020 Innsbruck, Austria[18]

C.K. Bowdery, T.J. Brodbeck, A.J. Finch, F. Foster, G. Hughes, D. Jackson, N.R. Keemer, M. Nuttall, A. Patel, T. Sloan, S.W. Snow, E.P. Whelan

Department of Physics, University of Lancaster, Lancaster LA1 4YB, United Kingdom[10]

A. Galla, A.M. Greene, K. Kleinknecht, J. Raab, B. Renk, H.-G. Sander, H. Schmidt, S.M. Walther, R. Wanke, B. Wolf

Institut für Physik, Universität Mainz, 55099 Mainz, Fed. Rep. of Germany[16]

A.M. Bencheikh, C. Benchouk, A. Bonissent, D. Calvet, J. Carr, C. Diaconu, F. Etienne, D. Nicod, P. Payre, L. Roos, D. Rousseau, M. Talby

Centre de Physique des Particules, Faculté des Sciences de Luminy, IN^{2}P^3-CNRS, 13288 Marseille, France

I. Abt, S. Adlung, R. Assmann, C. Bauer, W. Blum, D. Brown, P. Cattaneo,[23] B. Dehning, H. Dietl, F. Dydak,[21] A.W. Halley, K. Jakobs, H. Kroha, J. Lauber, D. Lehner,[28] G. Lütjens, G. Lutz, W. Männer, H.-G. Moser, R. Richter, J. Schröder, A.S. Schwarz, R. Settles, H. Seywerd, U. Stierlin,[2] U. Stiegler, R. St. Denis, G. Wolf

Max-Planck-Institut für Physik, Werner-Heisenberg-Institut, 80805 München, Fed. Rep. of Germany[16]

R. Alemany, J. Boucrot, O. Callot, A. Cordier, F. Courault, M. Davier, L. Duflot, J.-F. Grivaz, Ph. Heusse, M. Jacquet, P. Janot, D.W. Kim,[19] F. Le Diberder, J. Lefrançois, A.-M. Lutz, G. Musolino, I. Nikolic, H.J. Park, I.C. Park, M.-H. Schune, S. Simion, J.-J. Veillet, I. Videau

Laboratoire de l'Accélérateur Linéaire, Université de Paris-Sud, IN^{2}P^3-CNRS, 91405 Orsay Cedex, France

D. Abbaneo, G. Bagliesi, G. Batignani, S. Bettarini, U. Bottigli, C. Bozzi, G. Calderini, M. Carpinelli, M.A. Ciocci, V. Ciulli, R. Dell'Orso, I. Ferrante, F. Fidecaro, L. Foà,[1] F. Forti, A. Giassi, M.A. Giorgi, A. Gregorio, F. Ligabue, A. Lusiani, P.S. Marrocchesi, A. Messineo, G. Rizzo, G. Sanguinetti, A. Sciabà, P. Spagnolo, J. Steinberger, R. Tenchini,[21] G. Tonelli,[27] G. Triggiani, C. Vannini, P.G. Verdini, J. Walsh

Dipartimento di Fisica dell'Università, INFN Sezione di Pisa, e Scuola Normale Superiore, 56010 Pisa, Italy

A.P. Betteridge, Y. Gao, M.G. Green, D.L. Johnson, T. Medcalf, Ll.M. Mir, I.S. Quazi, J.A. Strong

Department of Physics, Royal Holloway & Bedford New College, University of London, Surrey TW20 OEX, United Kingdom[10]

V. Bertin, D.R. Botterill, R.W. Clifft, T.R. Edgecock, S. Haywood, M. Edwards, P. Maley, P.R. Norton, J.C. Thompson

Particle Physics Dept., Rutherford Appleton Laboratory, Chilton, Didcot, Oxon OX11 OQX, United Kingdom[10]

B. Bloch-Devaux, P. Colas, H. Duarte, S. Emery, W. Kozanecki, E. Lançon, M.C. Lemaire, E. Locci, B. Marx, P. Perez, J. Rander, J.-F. Renardy, A. Rosowsky, A. Roussarie, J.-P. Schuller, J. Schwindling, D. Si Mohand, A. Trabelsi, B. Vallage

CEA, DAPNIA/Service de Physique des Particules, CE-Saclay, 91191 Gif-sur-Yvette Cedex, France[17]

R.P. Johnson, A.M. Litke, G. Taylor, J. Wear

Institute for Particle Physics, University of California at Santa Cruz, Santa Cruz, CA 95064, USA[22]

A. Beddall, C.N. Booth, C. Boswell, S. Cartwright, F. Combley, I. Dawson, A. Koksal, M. Letho, M.W. Newton, C. Rankin, L.F. Thompson

Department of Physics, University of Sheffield, Sheffield S3 7RH, United Kingdom[10]

A. Böhrer, S. Brandt, G. Cowan, E. Feigl, C. Grupen, G. Lutters, J. Minguet-Rodriguez, F. Rivera,[26] P. Saraiva, U. Schäfer, L. Smolik

Fachbereich Physik, Universität Siegen, 57068 Siegen, Fed. Rep. of Germany[16]

L. Bosisio, R. Della Marina, G. Giannini, B. Gobbo, L. Pitis, F. Ragusa[20]

Dipartimento di Fisica, Università di Trieste e INFN Sezione di Trieste, 34127 Trieste, Italy

H. Kim, J. Rothberg, S. Wasserbaech

Experimental Elementary Particle Physics, University of Washington, WA 98195 Seattle, U.S.A.

S.R. Armstrong, L. Bellantoni, J.S. Conway,[24] P. Elmer, Z. Feng, D.P.S. Ferguson, Y.S. Gao, S. Gonzáles, J. Grahl, J.L. Harton, O.J. Hayes, H. Hu, P.A. McNamara III, J.M. Nachtman, W. Orejudos, Y.B. Pan, Y. Saadi, M. Schmitt, I. Scott, V. Sharma, J.D. Turk, A.M. Walsh, F.V. Weber,[1] T. Wildish, Sau Lan Wu, X. Wu, J.M. Yamartino, M. Zheng, G. Zobernig

Department of Physics, University of Wisconsin, Madison, WI 53706, USA[11]

---

[1] Now at CERN, 1211 Geneva 23, Switzerland.
[2] Deceased.
[3] Now at Harvard University, Cambridge, MA 02138, U.S.A.
[4] Also Istituto di Fisica Generale, Università di Torino, Torino, Italy.
[5] Also Istituto di Cosmo-Geofisica del C.N.R., Torino, Italy.
[6] Now at TSM Business School, Enschede, The Netherlands.
[7] Supported by CICYT, Spain.
[8] Supported by the National Science Foundation of China.
[9] Supported by the Danish Natural Science Research Council.
[10] Supported by the UK Science and Engineering Research Council.
[11] Supported by the US Department of Energy, contract DE-AC02-76ER00881.
[12] On leave from Universitat Autonoma de Barcelona, Barcelona, Spain.
[13] Supported by the US Department of Energy, contract DE-FG05-92ER40742.
[14] Supported by the US Department of Energy, contract DE-FC05-85ER250000.
[15] Permanent address: Universitat de Barcelona, 08208 Barcelona, Spain.
[16] Supported by the Bundesministerium für Forschung und Technologie, Fed. Rep. of Germany.
[17] Supported by the Direction des Sciences de la Matière, C.E.A.
[18] Supported by Fonds zur Förderung der wissenschaftlichen Forschung, Austria.
[19] Permanent address: Kangnung National University, Kangnung, Korea.
[20] Now at Dipartimento di Fisica, Università di Milano, Milano, Italy.
[21] Also at CERN, 1211 Geneva 23, Switzerland.
[22] Supported by the US Department of Energy, grant DE-FG03-92ER40689.
[23] Now at Università di Pavia, Pavia, Italy.
[24] Now at Rutgers University, Piscataway, NJ 08854, USA.
[25] Now at University of Pittsburgh, Pittsburgh, PA 15260, U.S.A.
[26] Partially supported by Colciencias, Colombia.
[27] Also at Istituto di Matematica e Fisica, Università di Sassari, Sassari, Italy.
[28] Now at DESY-IfH,15738 Zeuthen, Germany.

1 Introduction

Using the ALEPH data recorded in 1989 and 1990, corresponding to almost 200,000 hadronic Z decays, the four-fermion final state arising from the process $e^+e^- \to l^+l^-f\bar{f}$ (where l is a charged lepton and f a charged fermion) was analyzed in the four- or six-prong (also called llV) topology. An excess in the $\tau^+\tau^-f\bar{f}$ final state with respect to the $e^+e^-f\bar{f}$ and the $\mu^+\mu^-f\bar{f}$ final states was indicated with a probability at the percent level [1]. Since then the update of the ALEPH analysis with further statistics [2], and independent analyses carried out by the other LEP collaborations [3] have not upheld this indication.

With an integrated luminosity corresponding to almost two million hadronic Z decays, recorded by ALEPH until the end of 1993 (see Table 1), *i.e.* with a statistics ten times larger than in 1990, a detailed study of this higher order electroweak process has become possible. Although a special emphasis is given to the low multiplicity final states (Section 3), the study presented here is not restricted to this llV topology: it is extended to $l^+l^-q\bar{q}$ final states with higher multiplicity (Section 4) and to $\nu\bar{\nu}l^+l^-$ and $\nu\bar{\nu}q\bar{q}$ final states (Section 5).

$\sqrt{s}$ (GeV)	$Z \to q\bar{q}$	L (pb^{-1})
88.361	6577	1.34
89.419	99853	10.15
90.218	26042	1.42
91.234	1608626	52.68
92.078	34223	1.45
93.020	146717	10.49
93.928	13878	1.52
Total	1935910	79.05

Table 1. Efficiency corrected numbers of hadronic Z decays and integrated luminosities recorded by the ALEPH detector between 1989 and 1993, for centre-of-mass energies around the Z peak. Here, the luminosities have been determined from the number of multihadronic events, using in particular the total hadronic cross-section $\sigma_h^0 = 41.61$ nb taken from a combination of LEP measurements in Ref. [4].

A detailed description of the ALEPH detector can be found in Ref. [5], and of its performance in Ref. [6]. Charged particles are detected in the central part of the detector consisting of a precision vertex detector, a cylindrical drift chamber and a large time projection chamber, measuring altogether up to 31 coordinates along the charged particle trajectories. In the geometrical acceptance of the time projection chamber, down to typically 16° from the beam axis, the tracking efficiency is measured to be in excess of

99.9%. A 1.5 T axial magnetic field is provided by a superconducting solenoidal coil. A relative resolution on the transverse momentum of $6.10^{-4} p_T$ (p_T in GeV/c) is achieved. In the following, *good* tracks are defined as charged particle tracks reconstructed with at least four hits in the time projection chamber, originating from within a cylinder of length 20 cm and radius 2 cm coaxial with the beam and centred at the nominal collision point, and with a polar angle with respect to the beam such that $|\cos\theta| < 0.95$. Tracks that are reconstructed with at least four hits in the time projection chamber, but do not originate from the nominal collision point as described above, are called *bad* tracks.

In addition to its rôle as a tracking device, the time projection chamber also serves to separate charged particle species with the measurement by up to 330 sense wires of their specific energy loss by ionization, or $\mathrm{d}E/\mathrm{d}x$. This allows electrons to be separated from other charged particle species (muons, pions, kaons) by more than three standard deviations up to a momentum of 8 GeV/c.

Electrons (and photons) are also identified in the electromagnetic calorimeter, a 22 radiation length thick sandwich of lead planes and proportional wire chambers with fine read-out segmentation, by the characteristic longitudinal and transverse developments of their associated showers. The relative energy resolution achieved is $0.18/\sqrt{E}$ (E in GeV).

Muons are identified in the hadron calorimeter, a 1.5 m thick yoke interleaved with 23 layers of streamer tubes, together with two surrounding layers of muon chambers, by their characteristic penetration pattern. In association with the electromagnetic calorimeter, the hadron calorimeter also provides a measurement of the hadronic energy with a relative resolution of $0.80/\sqrt{E}$ (E in GeV).

Taus are identified in particular by the missing energy carried away by their decay neutrinos. The total visible energy is measured with an energy-flow reconstruction algorithm which combines all the above measurements, supplemented by the energy detected at low polar angle (down to 24 mrad from the beam axis) by two additional electromagnetic calorimeters, used for the luminosity determination. The relative resolution on the total visible energy is $0.60/\sqrt{E}$ for high multiplicity final states (such as hadronic Z decays) and $0.25/\sqrt{E}$ for final states of low multiplicity without neutral hadrons (such as radiative dilepton events). In addition to the total visible energy measurement, the energy-flow reconstruction algorithm also provides a list of charged and neutral reconstructed objects, called *energy-flow particles* in the following.

In the data sample used for the analysis reported here, all major components of the detector were required to be simultaneously operational, and all major trigger logic had to be enabled.

2 The Monte Carlo samples

The analysis is based on large Monte Carlo event samples for the four-fermion process and possible backgrounds, allowing both selective and efficient selection criteria to be designed. A particular care was taken over the four-fermion Monte Carlo program so that

reliable predictions of the total production cross-sections and of the event distributions could be made.

2.1 The four-fermion process

The four-fermion process was simulated using the four-fermion generator `FERMISV` [7] where all the lowest order diagrams involving neutral boson (γ and Z) exchange are included. These diagrams are separated in four gauge-invariant sub-groups called conversion, annihilation, Bremsstrahlung and multiperipheral diagrams (see Fig. 1). The two latter only contribute to final states containing electrons. The multiperipheral diagrams, responsible for the so-called two-photon collisions, present a huge pole which is not regularized in `FERMISV` when the two electrons escape in the beam pipe. For this reason, the final state electrons were generated only above a finite angle with respect to the beam direction. This reduces the multiperipheral diagram contribution to the percent level. Un-tagged two-photon collisions were therefore treated as an independent background.

Purely charged leptonic final states were generated with the initial state radiation enabled, and allowing up to four final state photons to be radiated. In final states containing electrons, all charged lepton directions were required to be more than 10° from the beam axis, and all the e^+e^- invariant masses had to exceed 20 MeV/c^2 in order to avoid generating events that would be rejected later by selection criteria against photon conversion (see Section 3.1.4).

For the final states involving a $q\bar{q}$ pair, some modifications were implemented into `FERMISV` in order to incorporate QCD corrections to the production rate. Since low mass $q\bar{q}$ pairs essentially arise from a virtual photon radiated by one of the initial or final lepton legs, the contribution of the corresponding diagrams can simply be corrected by the value of the ratio of the experimental $e^+e^- \rightarrow$ hadrons cross-section to the prediction of the quark-parton model, trivially related to the experimental ratio R. This includes:

- the resonant cross-section, with the ρ production parameterized as in Ref. [8], and all the $J^{PC} = 1^{--}$ narrow resonances up to the $\Upsilon(11020)$. These are treated with the Breit-Wigner formula

$$\sigma_{BW} = \frac{3\pi}{m_{q\bar{q}}} \frac{\Gamma_{tot}\Gamma_{e^+e^-}}{(m_{q\bar{q}} - m_0)^2 + \frac{\Gamma_{tot}^2}{4}},$$

  where $m_{q\bar{q}}$ is the $q\bar{q}$ pair invariant mass, and m_0, Γ_{tot} and $\Gamma_{e^+e^-}$ are the resonance mass, total width and partial decay width into e^+e^-, as taken from Ref. [9]. The ω's and the ρ's are associated to the $l^+l^-u\bar{u}$ and $l^+l^-d\bar{d}$ production according to the electric charge of the u and d quarks, the ϕ's to the $l^+l^-s\bar{s}$ production, the ψ's to the $l^+l^-c\bar{c}$ production and the Υ's to the $l^+l^-b\bar{b}$ production. The $1S$ and $2S$ states are then decayed according to their measured branching ratios [9]. The experimental accuracy of the pion form-factor and of the resonance parameter measurements turns into an uncertainty of $\pm 3\%$ on the number of $l^+l^-q\bar{q}$ events produced in this resonant sector;

- the contribution of the continuum, parameterized as described in Ref. [10] up to a $q\bar{q}$ mass of 40 GeV/c^2. To a first approximation, the attribution to each quark flavour is done proportionally to the first order QCD prediction of R, and the difference between the experimental value and this prediction is attributed to $b\bar{b}$ above the $b\bar{b}$ resonances, to $c\bar{c}$ between the ψ's and the Υ's and to $s\bar{s}$ between the ϕ's and the ψ's. The resulting correction on the $e^+e^- \to l^+l^-q\bar{q}$ cross-section remains below 10% for all the quark flavours. A systematic uncertainty of $\pm 5\%$ on this cross-section, corresponding to a 50% uncertainty on the correction, is conservatively assumed;

- an overall correction factor of $1 + \alpha_s(m^2_{q\bar{q}})/\pi$ for higher $q\bar{q}$ masses.

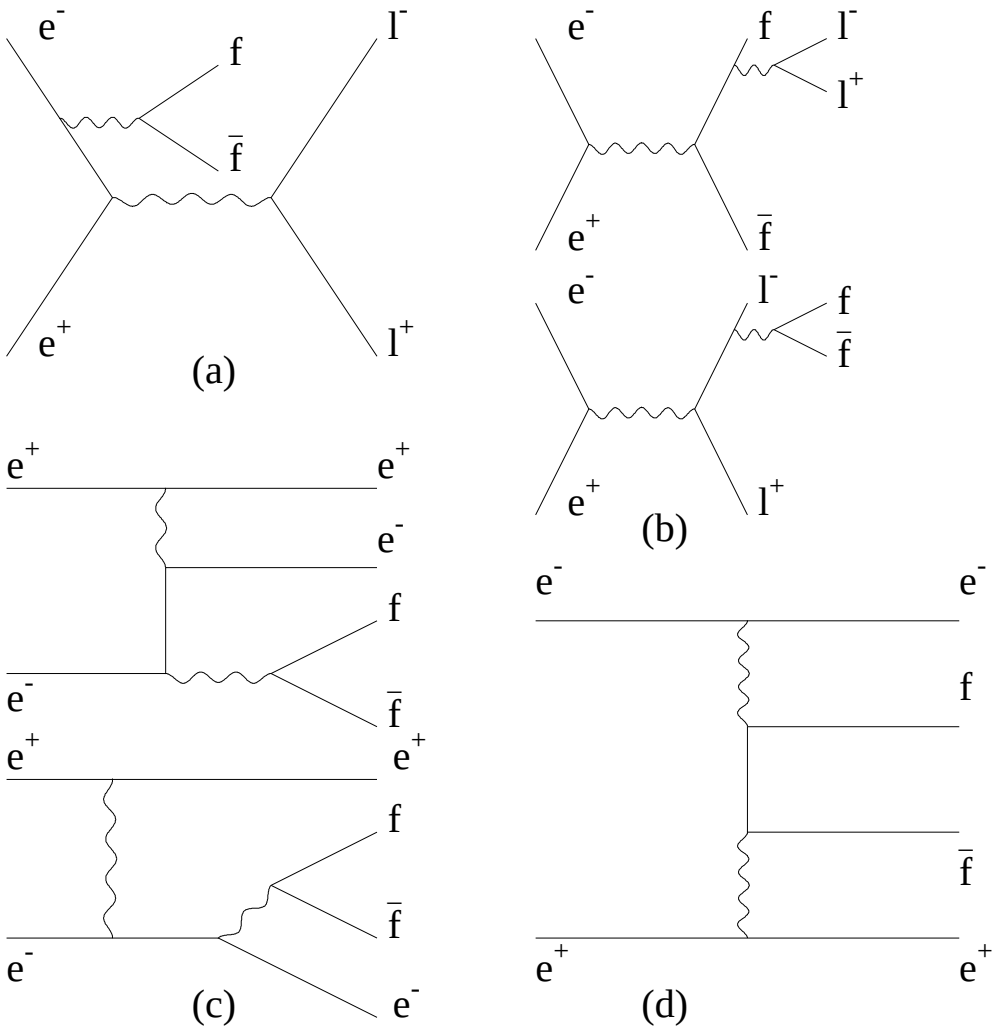

Figure 1: The four gauge-invariant groups of diagrams for the four-fermion production $e^+e^- \to l^+l^-f\bar{f}$: conversion (a), annihilation (b), Bremsstrahlung (c) and multiperipheral (d) diagrams. The wiggly lines represent γ or Z exchanges. The total cross-section is dominated by the diagrams of type (b). Similar graphs can be built by replacing the charged leptons by a neutrino pair, in which case the diagrams of type (a) dominate over diagrams of type (b).

No attempt was made to include QCD corrections for diagrams where the l^+l^- pair is radiated from a high mass pair of quarks. It has been shown for real photon emission [11] that gluon radiation (not simulated in FERMISV) competes with and tends to reduce the photon radiation by 30 to 50%. A systematic correction of $(-30 \pm 30)\%$ is therefore applied to the number of events predicted to predominantly arise from these diagrams. The effect of this correction is negligible in the llV topology.

Using this modified program, events were generated for all the possible $l^+l^-q\bar{q}$ final states, with initial state radiation enabled and allowing up to two final state photons to be radiated. When l = e, the lepton directions were required to be more than 15° from the beam axis, and the e^+e^- invariant mass had to exceed 200 MeV/c^2.

For all the final states, the cross-sections were computed at seven centre-of-mass energies around the Z peak with a statistical accuracy of 1% (see Table 2).

$f\bar{f} \longrightarrow$		e^+e^-	$\mu^+\mu^-$	$\tau^+\tau^-$	$d\bar{d}$	$u\bar{u}$	$s\bar{s}$	$c\bar{c}$	$b\bar{b}$
$l\bar{l}\downarrow$	$\sqrt{s}$								
	89.4	3.140	1.469	0.633	0.344	1.106	0.264	0.412	0.169
e^+e^-	91.2	4.053	2.883	1.601	0.729	2.085	0.615	1.044	0.374
(pb)	93.0	2.721	1.813	0.987	0.706	1.467	0.619	0.775	0.465
	89.4	1.469	0.207	0.194	0.214	0.559	0.186	0.303	0.134
$\mu^+\mu^-$	91.2	2.883	0.562	0.539	0.604	1.606	0.535	0.941	0.382
(pb)	93.0	1.813	0.339	0.324	0.655	1.138	0.591	0.742	0.519
	89.4	0.633	0.194	0.019	0.066	0.261	0.042	0.065	0.010
$\tau^+\tau^-$	91.2	1.601	0.539	0.053	0.181	0.707	0.114	0.191	0.028
(pb)	93.0	0.987	0.324	0.025	0.107	0.430	0.065	0.094	0.015
	89.4	162	30.6	0.5	7.8	31.1	3.7	1.5	0.2
$\nu_\mu\overline{\nu}_\mu$	91.2	591	95.7	0.8	22.1	87.4	9.6	2.5	0.7
(fb)	93.0	661	191	1.2	53.4	278	25.1	5.2	0.3

Table 2. Examples of production cross-sections for different four-fermion final states at $\sqrt{s}$ = 89.4, 91.2 and 93.0 GeV, as predicted by the modified FERMISV program.

For each of these final states, respectively 1000, 500 and 500 events were generated at $\sqrt{s}$ = 91.2, 89.4 and 93.0 GeV. Taus were decayed using KORALZ [12]. The $q\bar{q}$ fragmentation and hadronization, and the resonance decays were implemented using JETSET [13]. The events were then processed through the ALEPH simulation and reconstruction programs, and were used to determine the selection efficiencies. The efficiencies at different centre-of-mass energies were evaluated by linear extrapolation or interpolation.

2.2 The background processes

Large Monte Carlo samples of fully simulated and reconstructed events were produced for all the major background processes ($e^+e^- \to f\bar{f}$ and $\gamma\gamma \to f\bar{f}$, where $f\bar{f}$ is any quark or lepton pair):

- a sample of 1,500,000 hadronic Z decays, generated with `DYMU3` [14] interfaced with `JETSET` [13]; a sample of 350,000 $Z \to b\bar{b}$ events, equivalent to 1,600,000 hadronic Z decays; a sample of 47,000 $Z \to b\bar{b}$ events with two subsequent semi-leptonic decays, equivalent to 4,000,000 hadronic Z decays;
- a sample of 380,000 $Z \to \tau^+\tau^-$ decays corresponding to over four times the ALEPH data sample, generated with `KORALZ` [12];
- a sample of 185,000 dimuon events, with twice as many events as in the ALEPH data, generated with `KORALZ`;
- a sample of 100,000 Bhabha events generated with `UNIBAB` [15], and another sample of 150,000 events generated with `BABAMC` [16] with the two electron directions more than 15° from the beam axis, representing altogether approximately 1.5 times the recorded luminosity;
- large samples of two-photon events into hadrons, $\tau^+\tau^-$, $\mu^+\mu^-$ and e^+e^-, all corresponding to an integrated luminosity equivalent to or larger than the data, simulated according to QED for leptonic final states [17] and to both QPM and a VDM parameterization [18] for hadronic final states.

When necessary, and in order to have more Monte Carlo statistics, these samples were supplemented by large samples of events generated with a fast, but reasonably detailed, simulation of the ALEPH detector.

3 The llV topology selection

The llV topology corresponds to a four- or six-charged particle final state, and arises from the four-lepton production $e^+e^- \to e^+e^-e^+e^-$, $e^+e^-\mu^+\mu^-$, $e^+e^-\tau^+\tau^-$, $\mu^+\mu^-\mu^+\mu^-$, $\mu^+\mu^-\tau^+\tau^-$ and $\tau^+\tau^-\tau^+\tau^-$, or even from $e^+e^- \to l^+l^-q\bar{q}$, with $l = e$, μ or τ, when the mass of the quark-antiquark pair does not exceed a few GeV/c^2.

The selection criteria presented in Ref. [1] were tailored to an integrated luminosity of 8.6 pb^{-1}. In order to cope with the background expected in the 79 pb^{-1} now available, a more selective algorithm had to be developed and is described in the following.

3.1 The four-prong event selection

Only events with exactly four good charged particle tracks are considered in this section. The total electric charge is required to be zero and the energy measured below 12° from the beam axis has to be smaller than 1 GeV. The main backgrounds to this four-prong topology are:

(i) the $e^+e^- \to \tau^+\tau^-$ process, essentially in the 1 prong + 3 prong decay modes;

(ii) low multiplicity hadronic Z decays;

(iii) the two-photon collisions, especially $\gamma\gamma \to \tau^+\tau^-$ and $\gamma\gamma \to$ hadrons;

(iv) radiative dilepton events, with a photon conversion into an e^+e^- pair.

They have been eliminated by criteria chosen using the Monte Carlo samples listed in Section 2.2, as described in the following subsections.

3.1.1 $\tau^+\tau^-$ background

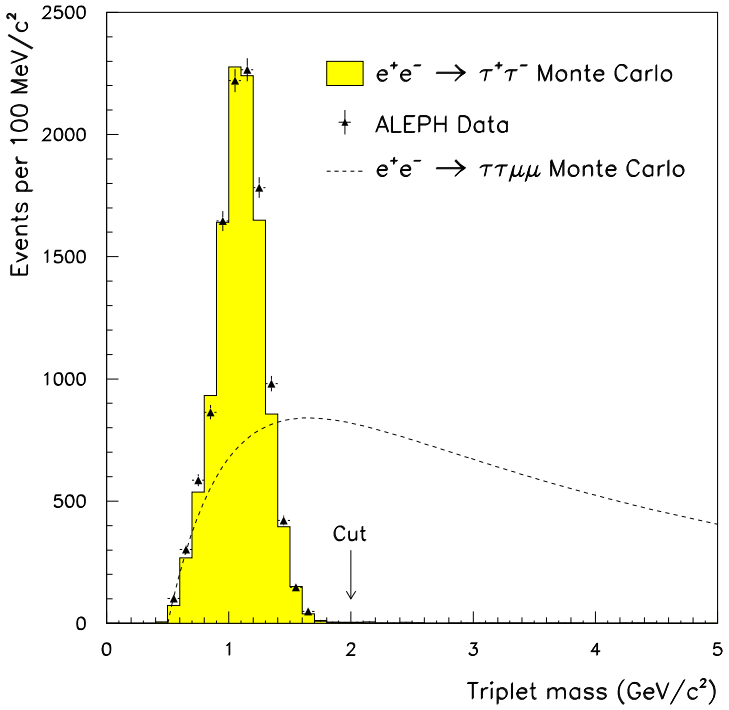

Figure 2: Distributions of the smallest triplet mass for events with four good tracks, in the ALEPH data (triangles with error bars), for the $e^+e^- \to \tau^+\tau^-$ Monte Carlo (shaded histogram, with an absolute normalization) and for the $e^+e^- \to \tau^+\tau^-\mu^+\mu^-$ Monte Carlo (dotted line, with an arbitrary normalization). The cut at 2 GeV/c^2 is indicated by an arrow.

As shown in Fig. 2, almost 99.9% of the $\tau^+\tau^-$ events in the 1 prong + 3 prong topology are rejected by requiring that all the triplets of electric charge ± 1 which can be formed with the four charged particles be not compatible with a τ, namely that they have an invariant mass in excess of 2 GeV/c^2.

Most of the 65 remaining $\tau^+\tau^-$ Monte Carlo events are affected by a nuclear interaction of one of the four charged particles when going through the beam pipe or the detector material. This often creates secondary particles in the final state and always renders less accurate the triplet mass determination. It is therefore required that the smallest triplet mass exceed 4 GeV/c^2 when the sum of the distances of closest approach to the beam of the three tracks is larger than 5 mm, and that the number of additional bad tracks be smaller than two. At this level, 2.6 ± 0.7 $\tau^+\tau^-$ events are still expected in the data. They are mostly from 3 prong + 3 prong decays when one charged particle is missed in each of the two event hemispheres. They are removed by imposing an invariant mass larger than 2 GeV/c^2 (determined from the charged particles only) in at least one of the two hemispheres defined by a plane perpendicular to the event thrust axis. After all these requirements, only $0.24^{+0.35}_{-0.15}$ events coming from the $e^+e^- \to \tau^+\tau^-$ process are predicted to remain in the data.

3.1.2 Hadronic Z decays

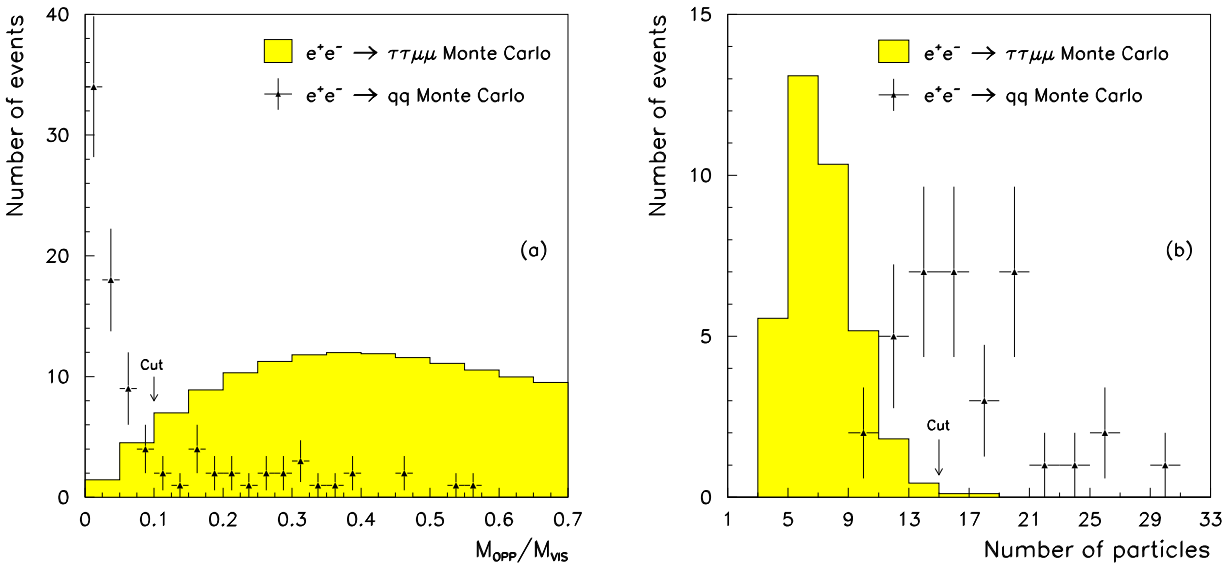

Figure 3: Distributions of the fraction of the visible mass carried by the pair recoiling against the smallest mass pair (a), and of the number of energy-flow particles after the first criterion is applied (b), for events with four good tracks, in the $e^+e^- \to q\bar{q}$ Monte Carlo (triangles with error bars, with an absolute normalization), and in the $e^+e^- \to \tau^+\tau^-\mu^+\mu^-$ final state (shaded histogram, with an arbitrary normalization). The cuts are indicated by an arrow.

The JETSET model predicts a few dozen low charged multiplicity hadronic Z decays, with a large fraction of the visible energy carried by neutral particles, in the four-fermion event sample. Most of these events are eliminated by requiring *(i)* that more than 10% of the visible mass be carried by the pair recoiling against the smallest mass pair of oppositely charged particles, and *(ii)* as suggested in Ref. [6], that the number of energy-flow particles not exceed fifteen. The distributions of these two quantities are shown in Fig. 3 both for the $e^+e^- \to q\bar{q}$ background and for the $e^+e^- \to \tau^+\tau^-\mu^+\mu^-$ final state. The few remaining events are removed in the classification stage (see Section 3.3) by requiring events with a total visible energy larger than $90\%\sqrt{s}$ to be identified as eeV or $\mu\mu$V. Altogether, $0.0^{+1.5}_{-0.0}$ hadronic Z decays are expected to remain in the data.

3.1.3 Two-photon collisions

Two-photon collisions are expected to produce events at low visible mass with large missing energy and momentum along the beam axis. They can be rejected by requiring *(i)* the missing transverse momentum to be larger than $5\%\sqrt{s}$ when the visible mass is below 25 GeV/c^2 (see Fig. 4) and *(ii)* the missing momentum along the beam direction not to exceed $35\%\sqrt{s}$. This latter cut also removes four-fermion events with hard initial state radiation, for which the total energy measurement could not be used for the event classification. After these criteria are applied, $0.0^{+0.6}_{-0.0}$ two-photon events are expected to remain in the data.

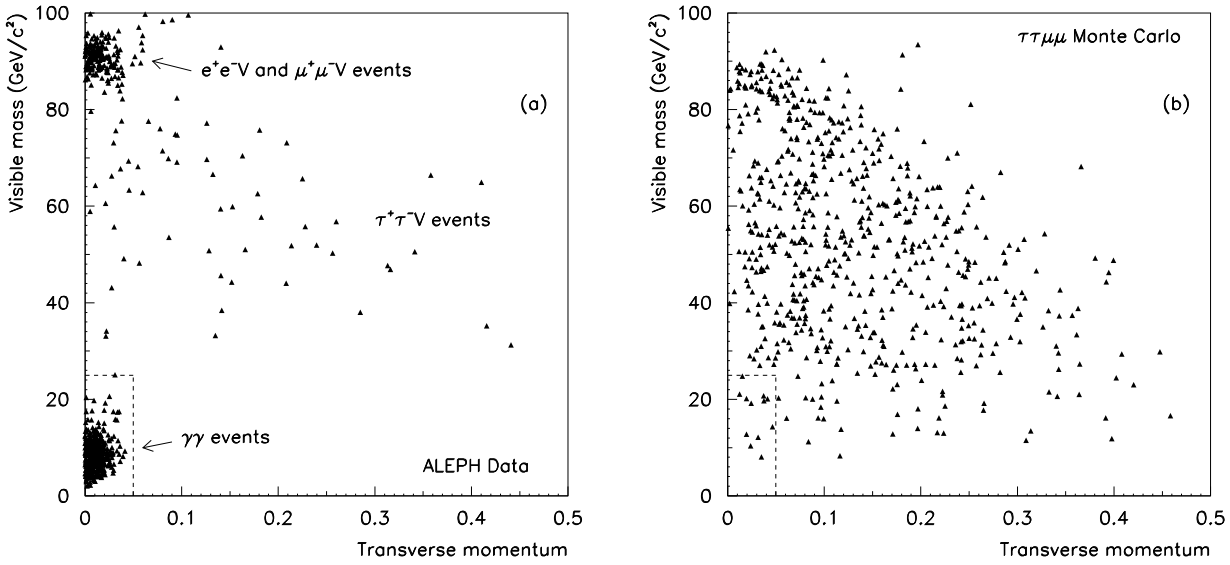

Figure 4: Distributions of the visible mass versus the total momentum transverse to the beam (in unit of the centre-of-mass energy) for the ALEPH data (a), and the $e^+e^- \to \tau^+\tau^-\mu^+\mu^-$ Monte Carlo (b). The cut performed in this plane is indicated by a dotted line.

3.1.4 $l^+l^-\gamma$ events

Finally, the hundreds of radiative dilepton events with a photon conversion in the detector material are rejected when the pair of oppositely charged particles with the smallest mass satisfies one of the following conditions: *(i)* the sum of the distances of closest approach to the beam of the two reconstructed tracks is larger than 5 mm; *(ii)* the invariant mass is smaller than 50 MeV/c^2, when calculated as for an e^+e^- pair coming from the main interaction point; *(iii)* the polar angle difference is smaller than 1° and the angle between the two directions (in space) is smaller than 8°, if the pair is identified as being e^+e^- (see Section 3.3); or *(iv)* the distance of closest approach of the two tracks is smaller than 1 mm and the invariant mass is smaller than 30 MeV/c^2, when calculated as for an e^+e^- pair coming from this point of closest approach. This leads to an expectation of $0.0^{+0.5}_{-0.0}$ radiative dilepton events selected as four-fermion final states in the data.

Altogether, the number of background events expected in the data is $0.24^{+1.70}_{-0.15}$. The overall efficiency of the selection amounts to $60.6 \pm 0.9\%$ for $e^+e^- \to \mu^+\mu^-\mu^+\mu^-$ events generated at $\sqrt{s} = 91.2$ GeV. This corresponds to an efficiency of $\sim 85\%$ in the TPC geometrical acceptance of 72%, the latter being defined as the fraction of $\mu\mu\mu\mu$ events with at least four good charged particle tracks.

3.2 The six-prong event selection

In order to improve the selection efficiency for four-fermion final states with taus (which, for instance, amounts to only 32% for $\tau\tau\mu\mu$ events if only the above selection criteria are used), the 1 prong + 3 prong decay mode of the τ pairs, leading to six-prong final states, have also been included in this study.

Events with exactly six good charged particle tracks, with a total electric charge zero and with an energy measured below 12° from the beam axis smaller than 1 GeV, are considered in this section. Since only events containing taus are concerned by this complementary selection, the total energy is required to be smaller than $85\%\sqrt{s}$. Furthermore, at least one charged particle triplet of total charge ± 1 must have a mass smaller than 1.8 GeV/c^2 and a total momentum in excess of 2 GeV/c. If more than one such triplet is found, only the most energetic one is selected as being a τ.

To reject tau pairs in the 3 prong + 3 prong topology, the opposite charged particle triplet must have an invariant mass larger than 2 GeV/$c^2$and, following the strategy of the previous section, larger than 4 GeV/c^2 when the sum of the distances of closest approach to the beam of the three tracks is larger than 5 mm. Tau pairs in the 1 prong + 5 prong decay modes are eliminated when a charged particle quintuplet of total electric charge ± 1 is found with a mass smaller than 2.5 GeV/c^2. When the sum of the distances of closest approach to the beam of the five tracks is larger than 2 cm, the cut value is increased to 5 GeV/c^2. The residual interactions with the detector material are avoided by requiring that the number of bad charged particle tracks be smaller than two. When these criteria are applied, $0^{+0.28}_{-0.0}e^+e^- \to \tau^+\tau^-$ events are expected to remain in the data.

No modifications to the previous strategy are needed to reduce the contamination from the other backgrounds (see Sections 3.1.2 to 3.1.4) down to an expectation of $0.0^{+1.7}_{-0.0}$ events. Once this complementary selection is included, the efficiency for $\tau\tau\mu\mu$ events increases from 32% to 43.5%. Other channels with taus have similar improvement.

3.3 The event classification

Since all the background contributions have been reduced down to a negligible level, the events satisfying the selection criteria listed in Sections 3.1 and 3.2 can be interpreted as coming exclusively from the four-fermion process $e^+e^- \to l^+l^-f\bar{f}$ where l is a charged lepton and f any charged fermion (lepton or quark). Two of these events are shown in Fig. 5 and Fig. 6, classified as $e^+e^-\mu^+\mu^-$ and $\tau^+\tau^-\mu^+\mu^-$ respectively.

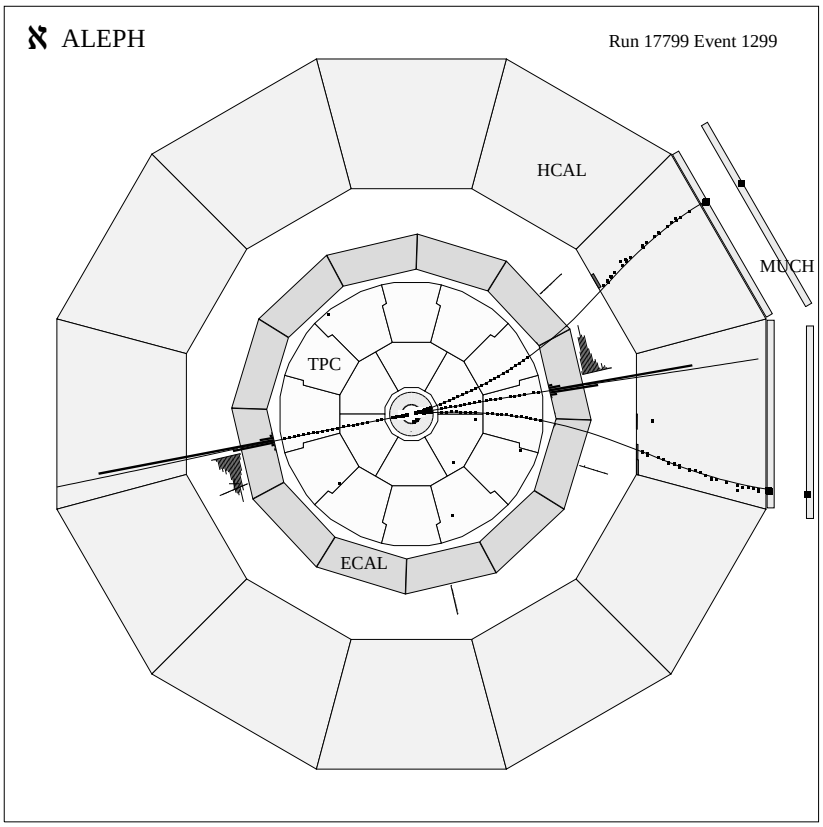

Figure 5: A $r\varphi$ view of the ALEPH detector for an event classified as $e^+e^- \to e^+e^-\mu^+\mu^-$. The Time Projection Chamber (TPC), the Electromagnetic CALorimeter (ECAL), the Hadron CALorimeter (HCAL) and the MUon CHambers (MUCH) are indicated.

To classify these events, the $f\bar{f}$ pair is defined as the smallest mass pair of oppositely charged particles, not belonging to the tau-triplet in the case of the six-prong topology. The l^+l^- pair, formed by the other charged particle tracks of the event, is identified using the missing energy measurement and the electron and muon identification capabilities of the ALEPH detector [6] as follows.

- Events with a total visible energy above $90\%\sqrt{s}$ and no lepton (e or μ) identified in the calorimeters are rejected, as already mentioned in Section 3.1.

- Events with a total visible energy above $90\%\sqrt{s}$ and with at least one electron (resp. one muon) identified in the electromagnetic (resp. hadron) calorimeter are classified as $e^+e^-f\bar{f}$ (resp. $\mu^+\mu^-f\bar{f}$).

- Events with a total visible energy above $80\%\sqrt{s}$ and two electrons (resp. two muons) identified in the electromagnetic (resp. hadron) calorimeter are classified as $e^+e^-f\bar{f}$ (resp. $\mu^+\mu^-f\bar{f}$). The same classification holds when only one of the two leptons is identified, provided that the other hits an uninstrumented zone of the relevant calorimeter.

- To account for the large forward-peaked contribution of the t-channel to the eeV cross-section, and as suggested by the $l^+l^-\gamma$ study detailed below, the two previous energy cuts are lowered to $80\%\sqrt{s}$ and $60\%\sqrt{s}$ for one and two electrons identified, respectively, if either $\cos\theta_- > 0.7$ or $\cos\theta_+ < -0.7$, where $\theta_\pm$ is the angle of the $e^\pm$ direction with respect to the incoming electron direction.

- All the other events are classified as $\tau^+\tau^-f\bar{f}$, as well as all the events selected in the six-prong topology.

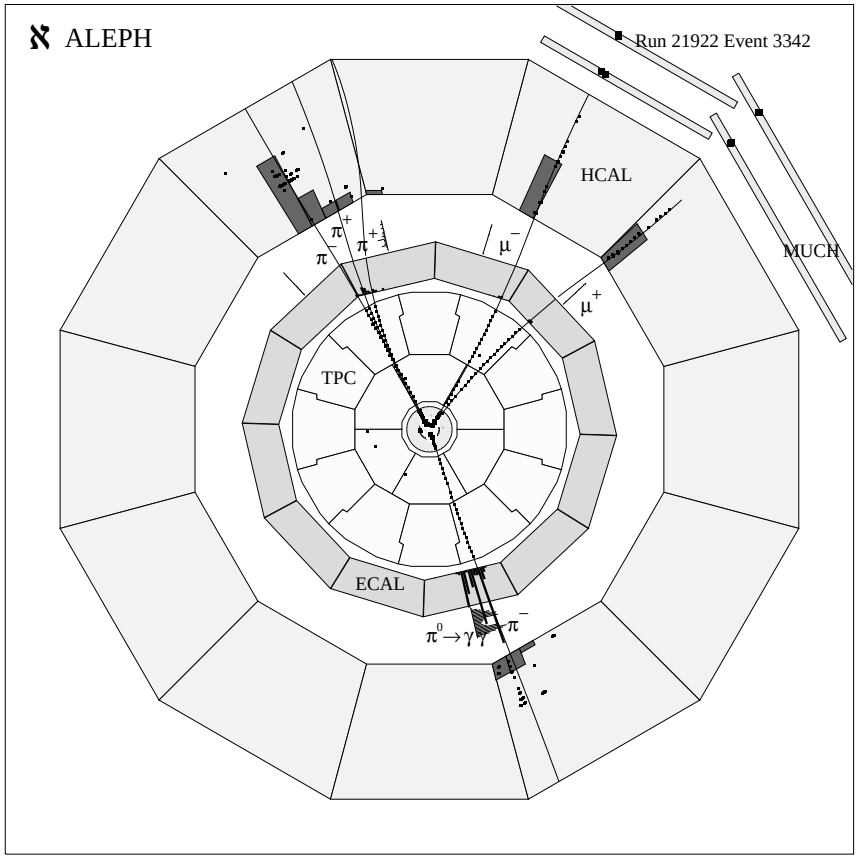

Figure 6: A $r\varphi$ view of the ALEPH detector for an event classified as $e^+e^- \to \tau^+\tau^-\mu^+\mu^-$ in the six-prong topology.

Both the missing energy measurement accuracy and the lepton identification efficiency are checked directly from the data using $l^+l^-\gamma$ events, where the l^+l^- pair is expected to have the same distributions (momenta, angles) as in $l^+l^-f\bar{f}$ final states. These events are selected as follows: *(i)* exactly two good charged particle tracks, *(ii)* at least one photon of energy larger than 2 GeV, *(iii)* the invariant masses formed by the photon and any of the two charged particles in excess of 2 GeV/c^2, and *(iv)* rejecting two-photon collisions and low multiplicity hadronic Z decays as indicated in Sections 3.1.2 and 3.1.3. A total of 14476 such events are selected in the data, in agreement with the prediction of the dilepton Monte Carlo generators. The observed total visible energy distribution, shown in Fig. 7, is in agreement with the expectation to an accuracy better than 0.5% for the total energy determination, turning into a precision better than 0.2% on the energy cut efficiencies deduced from the Monte Carlo, for the three lepton flavours.

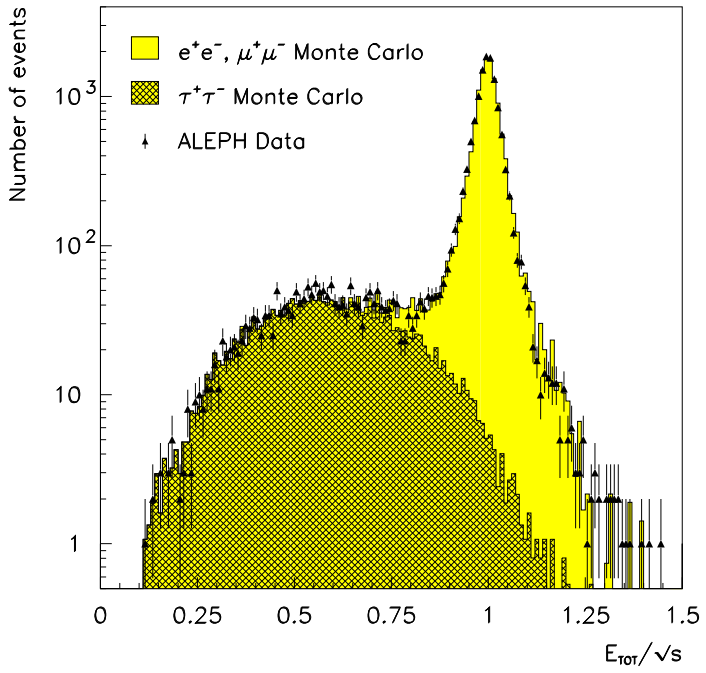

Figure 7: Distribution of the total visible energy for $l^+l^-\gamma$ events in the data (triangles with error bars) and the KORALZ + UNIBAB prediction normalized to the number of events observed (shaded histogram). The hatched area shows the expected contribution from $\tau^+\tau^-\gamma$ events.

For the lepton identification, $l^+l^-\gamma$ events with a total visible energy in excess of $90\%\sqrt{s}$ are used. This sample can be strongly enriched in Bhabha and dimuon events by requiring in addition the presence of an identified electron or muon on one side. A total of 7120 electron events and 4749 muon events are selected in the data. The residual background of $\tau^+\tau^-$ events is evaluated from Monte Carlo and amounts to 19 events in the electron sample and 12 events in the muon sample. After background subtraction, the other lepton of these events can therefore be used to determine the lepton identification efficiency, both in data and Monte Carlo. The results are shown in Table 3.

	Data				Monte Carlo			
	ε_{11}	ε'_{11}	ε_{21}	ε_{22}	ε_{11}	ε'_{11}	ε_{21}	ε_{22}
Muons	90.7	96.3	99.1	92.5	91.0	95.9	99.2	91.7
Electrons	82.1	98.2	96.8	93.9	84.1	99.0	97.5	95.6

Table 3. Lepton identifications efficiencies, in percent, as measured for the data and the Monte Carlo with radiative Bhabha and dimuon events, with a statistical uncertainty of 0.3%. ε_{11} is the probability for one lepton to be identified in the relevant calorimeter; in ε'_{11}, the lepton is also allowed to hit an uninstrumented calorimeter region; ε_{21} is the probability to identify one of two leptons; ε_{22} is the probability to identify both leptons of a pair, allowing one of the two to hit an uninstrumented calorimeter region.

For the $\mathrm{l^+l^-f\bar{f}}$ event classification, it turns out that the relevant efficiency is ε_{21}. It can be seen in Table 3 that the Monte Carlo overestimates the $\mathrm{e^+e^-}$ identification by $0.7\pm0.3\%$, while the $\mu^+\mu^-$ identification is adequately simulated. The proportion of events rejected by the first classification criterion amounts to 5.5%, 3.2% and 0.9% for $\tau^+\tau^-\gamma$, $\mathrm{e^+e^-}\gamma$ and $\mu^+\mu^-\gamma$ respectively. Finally, the cross-channel contamination is estimated to be at the level of 0.5% from $\tau^+\tau^-\gamma$ events to radiative Bhabha or dimuon events, 0.5% from $\mathrm{e^+e^-}\gamma$ and $\mu^+\mu^-\gamma$ to $\tau^+\tau^-\gamma$ events, and smaller than 0.01% between $\mathrm{e^+e^-}\gamma$ and $\mu^+\mu^-\gamma$.

The identification of the smallest mass pair of oppositely charged particles (the $\mathrm{f\bar{f}}$ pair) makes use both of the calorimeters and of the energy losses by ionization (also called $\mathrm{d}E/\mathrm{d}x$) measured by the TPC, particularly useful in the low momentum region. For $\mathrm{d}E/\mathrm{d}x$, four estimators (χ^i_e, χ^i_μ, χ^i_π and χ^i_K) are built. They are defined as the ratio of the difference between the measured energy loss $I^{i(meas)}$ and the expectation $I^{i(exp)}_x$ for the four mass hypotheses ($\mathrm{x} = \mathrm{e}, \mu, \pi, \mathrm{K}$), to the expected uncertainty $\sigma^{i(exp)}_x$ on this measurement, for each of the two tracks i of the pair:

$$\chi^i_x = \frac{I^{i(meas)} - I^{i(exp)}_x}{\sigma^{i(exp)}_x}.$$

The compatibility of the $\mathrm{f\bar{f}}$ pair with the hypothesis $\mathrm{x^+x^-}$ is therefore quantified by $(\chi_x)^2 \equiv (\chi^1_x)^2 + (\chi^2_x)^2$. The identification of the $\mathrm{f\bar{f}}$ pair is performed as follows.

- If at least one of the two charged particles is identified in the relevant calorimeter to be an electron or a muon as explained above, the $\mathrm{f\bar{f}}$ pair is classified as a $\mathrm{e^+e^-}$ or a $\mu^+\mu^-$ pair, respectively.

- If no lepton is identified although at least one of the two charged particles has a momentum larger than 1.5 GeV/c^2 (thus making it identifiable in the calorimeters), the pair is classified as $\pi^+\pi^-$, $\mathrm{K^+K^-}$ or $\tau^+\tau^-$, unless $\chi^2_e < \chi^2_{\pi,\mathrm{K}} - 3$, in which case the pair is classified as $\mathrm{e^+e^-}$.

  No attempt has been made yet to distinguish $\tau^+\tau^-$ and hadron pairs. However, due to the small number of $\tau^+\tau^-$ and $\mathrm{K^+K^-}$ pairs expected, all of them are called $\pi^+\pi^-$

in the following, unless $\chi^2_{\rm K} < \chi^2_\pi$ and the $\rm f\bar{f}$ mass computed in the $\rm K^+K^-$ hypothesis is well compatible with the ϕ mass ($1.01\ {\rm GeV}/c^2 < m_{\rm KK} < 1.06\ {\rm GeV}/c^2$), in which case the pair is classified as $\rm K^+K^-$.

- If the two charged particle momenta are smaller than $1.5\ {\rm GeV}/c^2$, the identification relies exclusively on the ${\rm d}E/{\rm d}x$ measurement: if the smallest χ^2 is obtained with the electron hypothesis, the pair is classified as $\rm e^+e^-$; if it is obtained with the kaon hypothesis and if the $\rm f\bar{f}$ mass is compatible with the ϕ mass, the pair is classified as $\rm K^+K^-$; otherwise, due to the small mass difference between the muon and the pion, the pair is classified as $\pi^+\pi^-$ or $\mu^+\mu^-$.

The efficiencies are determined from the four-fermion final state Monte-Carlo and are shown in Table 4. Since the ${\rm d}E/{\rm d}x$ measurement is used for only 15% of the events, an inadequacy of its simulation at the level of 10% would translate into an uncertainty of only 1.5% in the distinction $\rm e^+e^-/\pi^+\pi^-$ or $\mu^+\mu^-/\rm K^+K^-$, equivalent to the statistical uncertainty caused by the limited number of Monte Carlo events. No systematic checks of this ${\rm d}E/{\rm d}x$ simulation were therefore performed for this analysis.

$\rm f\bar{f} \longrightarrow$ Class $\downarrow$	$\rm e^+e^-$	$\mu^+\mu^-$	$\tau^+\tau^-$	$\rm d\bar{d}/u\bar{u}$	$\rm s\bar{s}$	$\rm c\bar{c}$	$\rm b\bar{b}$
$\rm e^+e^-$	**>99.5**	0.1	29.3	3.0	2.4	22.8	~ 50
$\mu^+\mu^-$	–	**78.8**	27.2	3.1	5.7	22.2	~ 50
$\pi^+\pi^-$	–	3.8	35.6	**77.1**	47.7	43.7	–
$\pi^+\pi^-$ or $\mu^+\mu^-$	–	**17.2**	7.9	**16.5**	6.0	11.1	–
$\rm K^+K^-$	–	0.1	–	0.3	**38.2**	–	–

Table 4. Efficiencies, in percent, of the smallest mass pair classification in $\rm e^+e^-$, $\mu^+\mu^-$, $\pi^+\pi^-$ or $\rm K^+K^-$ as a function of the $\rm f\bar{f}$ flavour generated. Events selected from the $\rm l^+l^-s\bar{s}$, $\rm l^+l^-c\bar{c}$ and $\rm l^+l^-b\bar{b}$ processes are dominated by the low multiplicity decays of the $1S$ and $2S$ resonances (ϕ, J/ψ and Υ).

3.4 The numbers of events expected

As a result of the above study, the overall efficiencies determined at $\sqrt{s} = 91.2$ GeV for the four- and six-prong topology selection criteria are

- 12.5% in the $\rm e^+e^-e^+e^-$ channel,
- 30.8% in the $\rm e^+e^-\mu^+\mu^-$ channel to be split into 17.1% in the eexx class (when the pair with the smallest mass is the $\mu^+\mu^-$ pair) and 13.7% in the $\mu\mu$xx class (when the pair with the smallest mass is the $\rm e^+e^-$ pair),

- 15.9% in the $e^+e^-\tau^+\tau^-$ channel to be split into 13.7% in the $\tau\tau$xx class and 2.2% in the eexx class,
- 60.6% in the $\mu^+\mu^-\mu^+\mu^-$ channel,
- 43.4% in the $\mu^+\mu^-\tau^+\tau^-$ channel to be split into 40.0% in the $\tau\tau$xx class and 3.4% in the $\mu\mu$xx class,
- 31.4% in the $\tau^+\tau^-\tau^+\tau^-$ channel,
- 14.2%, 11.5% and 23.9% in the $e^+e^-d\bar{d}$, the $\mu^+\mu^-d\bar{d}$ and $\tau^+\tau^-d\bar{d}$ channels,
- 18.8%, 19.7% and 25.0% in the $e^+e^-u\bar{u}$, the $\mu^+\mu^-u\bar{u}$ and $\tau^+\tau^-u\bar{u}$ channels,
- 7.7%, 4.4% and 6.4% in the $e^+e^-s\bar{s}$, the $\mu^+\mu^-s\bar{s}$ and $\tau^+\tau^-s\bar{s}$ channels,
- 1.3%, 1.4% and 4.5% in the $e^+e^-c\bar{c}$, the $\mu^+\mu^-c\bar{c}$ and $\tau^+\tau^-c\bar{c}$ channels,
- $\sim 0.1\%$ in the $l^+l^-b\bar{b}$ channels.

The apparently small values obtained for the final-states containing a e^+e^- or a $q\bar{q}$ pair are due to the poles of the cross-section at low e^+e^- invariant mass, and to the requirement that the $q\bar{q}$ pair hadronizes into two charged particles only. Using these efficiencies, the four-fermion process cross-sections detailed in Section 2.1 and the total integrated luminosities recorded by ALEPH at the various centre-of-mass energies, shown in Table 1, it is possible to determine the numbers of events expected in the data in the fifteen different llV classes. These numbers are shown in Table 5. The various systematic uncertainties on these numbers can be listed as follows.

1. Knowledge of $\sin^2\theta_W^{\rm eff}$ (0.2324 ± 0.0006, as determined from a combination of the four LEP experiments [4]): $\pm 0.5\%$;
2. Statistical accuracy of the total cross-section Monte Carlo computation: $\pm 1\%$;
3. Efficiency determination from the limited Monte-Carlo statistics: $\pm 1.5\%$;
4. Integrated luminosity determination at each centre-of-mass energy from the number of hadronic Z decays: $\pm 1\%$;
5. Inadequacy of the lepton identification simulation (essentially from the dE/dx for which no systematic checks have been performed here): $\pm 1.5\%$;
6. Missing higher order QED corrections, especially for the initial state radiation; this has been estimated by substituting the initial state photon energy spectrum of Ref. [19] for the simplified formula used in `FERMISV`: $\pm 1\%$;
7. For the $l^+l^-q\bar{q}$ channels, accuracy of the simulation of the resonances (dominated by the ρ) and of the R ratio: $\pm 4\%$.

Many other uncertainties at a much lower level, such as the knowledge of the QED coupling constant at the Z pole ($\pm 0.2\%$), the accuracy of the total energy simulation ($\pm 0.2\%$) or the Z mass and width values ($\pm 0.1\%$), result in an uncertainty which does not exceed 1%. To summarize, a systematic uncertainty smaller than $\pm 3\%$ affects the purely leptonic channels. It increases to $\pm 5\%$ for the $l^+l^-q\bar{q}$ processes. Altogether, when the correlated and uncorrelated uncertainties are accounted for, the total number of four-fermion events in the four- and six-prong topologies expected in the ALEPH data is 231.9 ± 4.7 (syst.).

	$e^+e^-x^+x^-$	$\mu^+\mu^-x^+x^-$	$\tau^+\tau^-x^+x^-$	Total
x = e	37.7 ± 1.2	25.9 ± 0.8	14.6 ± 0.5	78.2 ± 2.0
x = μ	29.1 ± 0.9	20.0 ± 0.6	12.9 ± 0.4	62.0 ± 1.5
x = π	30.7 ± 1.6	21.6 ± 1.1	13.1 ± 0.7	65.4 ± 3.1
x = π or μ	11.0 ± 0.4	8.4 ± 0.3	4.5 ± 0.2	23.9 ± 0.8
x = K	1.2 ± 0.05	0.8 ± 0.04	0.4 ± 0.02	2.4 ± 0.1
Total	109.7 ± 2.8	76.7 ± 1.9	45.5 ± 1.2	231.9 ± 4.7

Table 5. Number of events expected in the ALEPH data in the fifteen different llV classes, with the systematic uncertainties.

3.5 The data sample

The total number of events expected, 231.9 ± 4.7, is to be compared to the 229 events selected in the data, the details of which are shown in Table 6.

	$e^+e^-x^+x^-$	$\mu^+\mu^-x^+x^-$	$\tau^+\tau^-x^+x^-$	Total
x = e	23	34	13	68
x = μ	35	20	15	72
x = π	28	24	13	65
x = π or μ	11	7	4	22
x = K	2	0	0	2
Total	101	83	45	229

Table 6. Number of events observed in the fifteen different llV classes.

The comparison of the two series of numbers may trigger several observations:

- The 45 $\tau^+\tau^-$V events, of which 14 are found in the six-prong topology, are in agreement with the 45.5 ± 1.2 events expected. This agreement is consistent over all the five classes. The indication of an excess observed in the ALEPH 1989-1990 data is not confirmed. When the present analysis is restricted to these data, the number of events observed is 9 e^+e^-V, 11 $\mu^+\mu^-$V and 12 $\tau^+\tau^-$V, while 11.5 ± 0.4, 7.9 ± 0.3 and 4.6 ± 0.3 are expected respectively.

- The agreement is satisfactory in all the classes, with a χ^2 of 10.2 for 12 degrees of freedom, after the x=π and the x=K classes are merged. The largest discrepancy is observed in the $e^+e^-e^+e^-$ final state, where 23 events are observed for 37.7 ± 1.2 events expected. Whether this deficit of $e^+e^-e^+e^-$ events is due to a statistical fluctuation (at the 2.5σ level, expected to occur with a probability of 14% within 12 independent measurements) or results from, for instance, the absence of higher order QED corrections in `FERMISV` would require more data and more investigation to decide.

- After the inclusion of the $J^{PC} = 1^{--}$ resonances and the experimental ratio R, `FERMISV` reproduces well the number of $l^+l^-\pi^+\pi^-$ events (65 events observed, 65.4 expected) and of $l^+l^-K^+K^-$ events (2 events observed, 2.4 expected). The distribution of the $\pi^+\pi^-$ mass in $e^+e^- \to l^+l^-\pi^+\pi^-$ events is shown in Fig. 8a and agrees too with the modified `FERMISV` prediction.

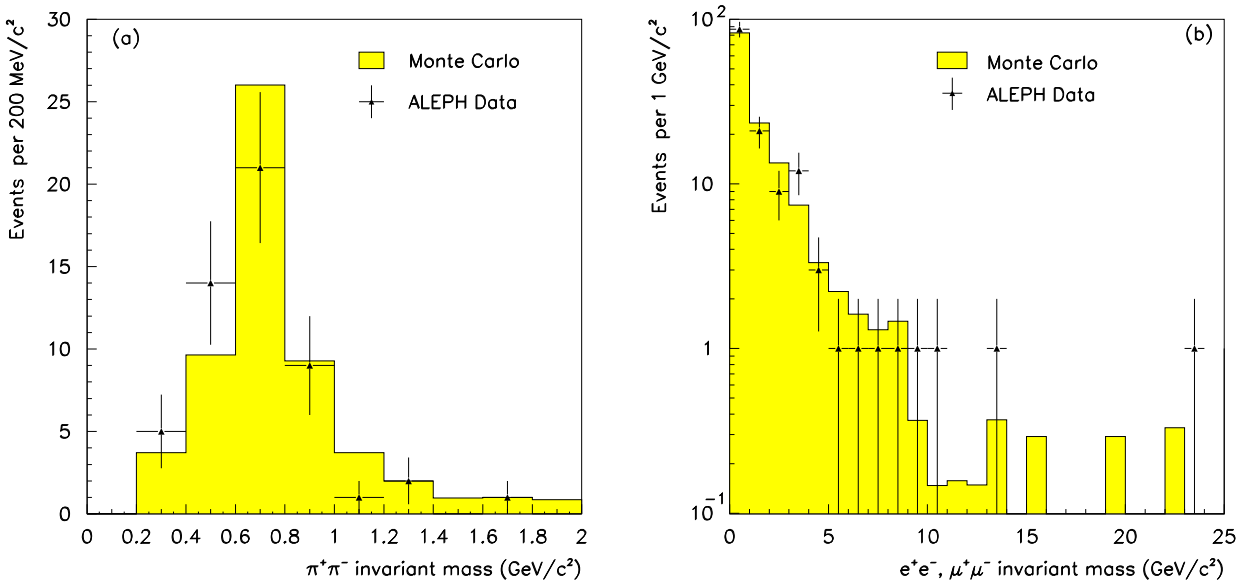

Figure 8: Distributions of the x^+x^- mass when x = π (a) and when x = e or μ (b), for the data (triangles with error bars) and for the Monte Carlo expectation (shaded histogram) with an absolute normalization.

Beyond the production rates, the distribution of the events in the multidimensional phase space can be compared with the standard model expectation. For that purpose,

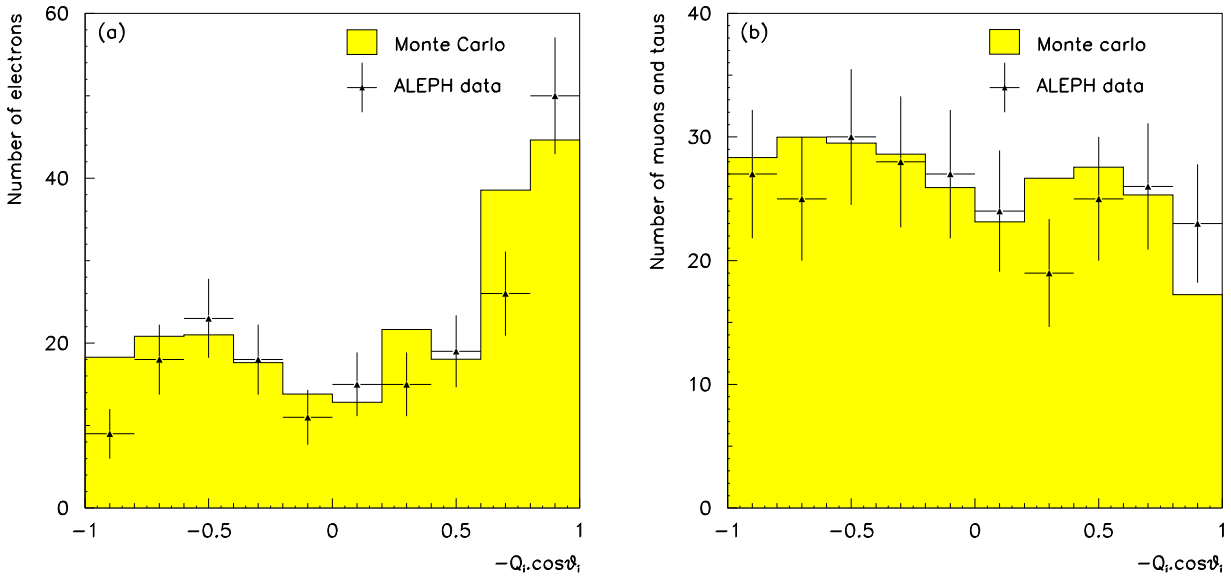

Figure 9: Angular distributions of the leptons (electric charge $\times$ cos[polar angle]) in the $e^+e^-x^+x^-$ final state (a) and in the $\mu^+\mu^-x^+x^-$ or $\tau^+\tau^-x^+x^-$ final states (b), for the data (triangles with error bars) and for the Monte Carlo expectation (shaded histogram) with an absolute normalization. Each event enters twice in the distributions.

several individual distributions can be examined such as the distribution of the $f\bar{f}$ pair mass, when identified as e^+e^- or $\mu^+\mu^-$ (see Fig. 8b), or the angular distributions of the leptons of the l^+l^- pair (see Fig. 9).

Ignoring the initial and final state radiated photons, the four-fermion final state is described by seven relevant kinematic variables. A systematic comparison of all distributions with the standard model prediction would be quite complicated, and not necessarily very powerful given the limited event statistics. A global and powerful test is obtained by constructing for each event i the normalized likelihood

$$p_i = \frac{\overline{|M_i|^2}}{\sigma_{tot}},$$

where $\overline{|M_i|^2}$ is the matrix element squared summed over all the possible fermion helicities as computed by `FERMISV` from the four-momenta of the four fermions, and σ_{tot} is the total cross-section expected for the corresponding final state.

To ensure both good knowledge of the event kinematics and accurate theoretical predictions, only events classified as $e^+e^-e^+e^-$, $e^+e^-\mu^+\mu^-$ or $\mu^+\mu^-\mu^+\mu^-$ were considered here. Furthermore, to reject residual $l^+l^-\pi^+\pi^-$ events wrongly identified as four-lepton events (see Table 4) and clustered around the ρ mass (see Fig. 8a), only 43 events found with a V mass in excess of 1 GeV/c^2 were kept; of these 7 are $e^+e^-e^+e^-$, 21 are $e^+e^-\mu^+\mu^-$ and 15 are $\mu^+\mu^-\mu^+\mu^-$.

The distribution of the normalized likelihood is shown in Fig. 10. Good agreement is found between data and Monte Carlo. In the standard model, the four-fermion matrix

element squared depends sensitively on the effective weak mixing angle $\sin^2\theta_{\rm W}^{\rm eff}$. A measure of $\sin^2\theta_{\rm W}^{\rm eff}$ can thus be obtained by maximizing the log-likelihood function

$$\mathrm{L}(\sin^2\theta_{\rm W}^{\rm eff}) = \sum_{i=1}^{N} \ln p_i(\sin^2\theta_{\rm W}^{\rm eff}),$$

where N is the total number of events considered in the procedure. (This is equivalent to maximizing the mean value of the distribution of Fig. 10.) With this method, a value of $\sin^2\theta_{\rm W}^{\rm eff} = 0.260 \pm 0.039$ (stat. only) is derived from the data.

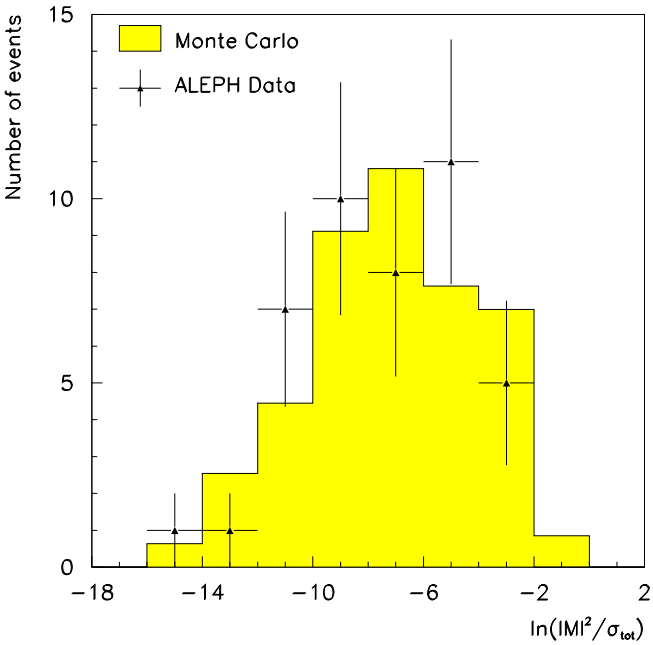

Figure 10: Distribution of $\ln p_i$, the normalized log-likelihood (see text), for $e^+e^-e^+e^-$, $e^+e^-\mu^+\mu^-$ and $\mu^+\mu^-\mu^+\mu^-$ events, in the data (triangles with error bars) and in the Monte Carlo (shaded area).

Within the still limited statistics, the four-fermion final state therefore shows good agreement with the standard model prediction both in shape and normalization.

4 The $l^+l^-q\bar{q}$ final state

The $l^+l^-q\bar{q}$ final state has partly been investigated in the previous section, when the $q\bar{q}$ system turns into a resonance that decays into two charged particles (essentially the ρ and the ω, but also the ϕ and the J/ψ for which 2.5 and 0.9 events are expected to be detected in the llV topology).

To study the continuum, for hadronic masses up to 70 GeV/c^2, another analysis is used which was developed initially for the Higgs boson search in the $e^+e^- \to HZ^* \to$ hadrons l^+l^- process [20]. This search essentially consists of selecting events with at least

six good charged particle tracks, of which two are energetic, isolated, identified electrons or muons. No events are selected in either of the hadronic Z decay Monte Carlo samples enriched in $b\bar{b}$ events of Section 2.2, equivalent to more than seven million Z decays, corresponding to $0.0^{+0.4}_{-0.0}$ background events expected in the data.

The numbers of four-fermion events expected in the ALEPH data are presented in Table 7, including the $l^+l^-\tau^+\tau^-$ background.

	f=d	f=u	f=s	f=c	f=b	f=τ	Total
$e^+e^-f\bar{f}$	1.79	5.97	1.07	4.95	0.49	0.54	14.81
$\mu^+\mu^-f\bar{f}$	1.87	5.43	1.10	4.46	0.55	0.22	13.63
$\tau^+\tau^-f\bar{f}$	0.01	0.07	0.01	0.08	0.01	0.00	0.18

Table 7. Numbers of events predicted in the selected $l^+l^-f\bar{f}$ final states.

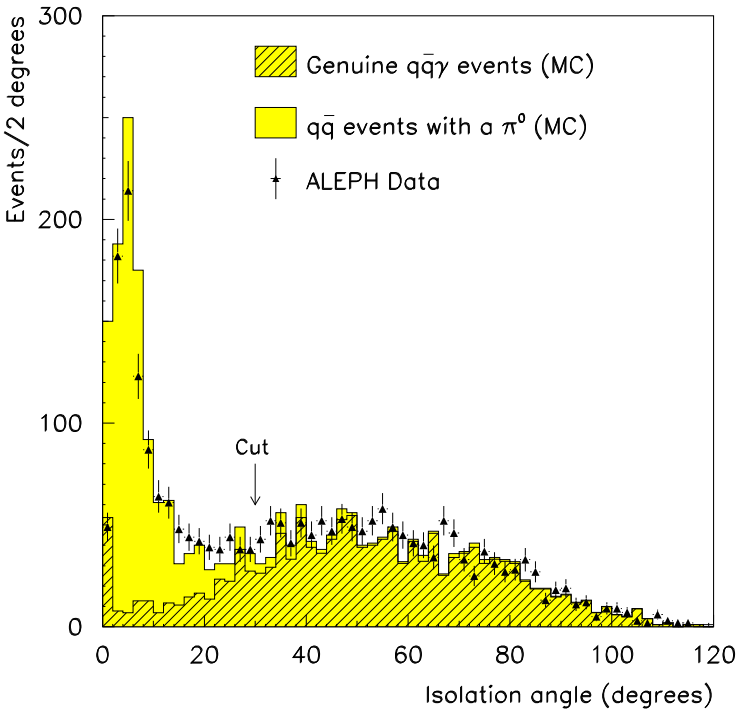

Figure 11: Distributions of the photon isolation angle, for the ALEPH data (triangles with error bars), and for the Monte Carlo (shaded histogram, with an absolute normalization). The isolation angle is defined as the angle of the largest cone around the photon direction containing less than 1 GeV of extra energy. The hatched part of the distribution is obtained from the genuine $q\bar{q}\gamma$ events. The cut at 30 degrees (applied to $l^+l^-q\bar{q}$ events too) is indicated by an arrow.

The systematic uncertainties on these numbers are expected to be rather small since most of the selection criteria rely only on the properties of very energetic and well isolated leptons for which the ALEPH simulation is known to be accurate.

However, the efficiency of the isolation criterion has been questioned in the past [11]. It has been checked with hadronic events containing a very energetic photon originating either from the radiative process $e^+e^- \to q\bar{q}\gamma$ or from the decay of an energetic π^0 in one of the jets. The selection of these events is very close to the $l^+l^-q\bar{q}$ selection, the photon playing the rôle of the lepton pair. In particular, its energy is required to be greater than 15 GeV and its transverse momentum with respect to the thrust axis of the rest of the event has to exceed 10 GeV/c. A total of 2542 such events are predicted by `JETSET` and 2423 are observed in the data.

As shown in Fig. 11, the photons of the genuine $q\bar{q}\gamma$ events tend to be isolated from the two jets due the transverse momentum cut. For photons coming from π^0 decays, this last cut *a priori* selects three-jet events, where one of the jets contains the energetic π^0, making it not isolated. The distribution of the photon isolation angle is well reproduced by the Monte Carlo both in shape and in normalization, thus giving confidence in the simulation of this quantity for the leptons.

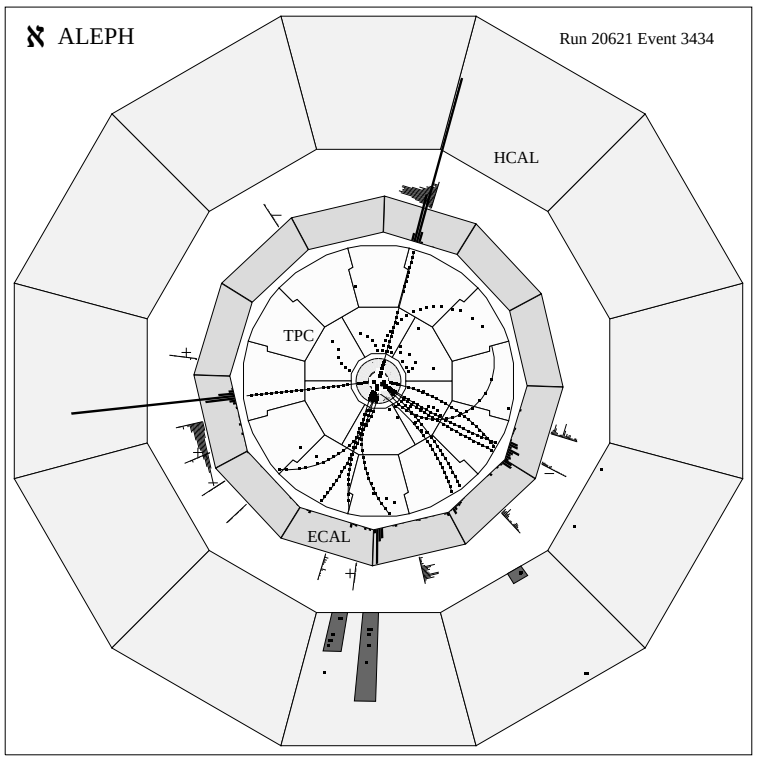

Figure 12: A $r\varphi$ view of the ALEPH detector for an $e^+e^- \to e^+e^-q\bar{q}$ event.

The major source of systematic uncertainty is therefore the absence, in the simulation, of QCD corrections for high $q\bar{q}$ masses, which could reduce the number of events expected in this region by 30% to 50% (see Section 2.1). The 4.7 events predicted by `FERMISV` with a hadronic mass above 40 GeV/c^2 have therefore to be corrected for a systematic bias of

-1.4 ± 1.4 events, leading to 3.3 ± 1.4 events expected. For lower masses, a 5% uncertainty mainly related to the experimental R ratio turns into an uncertainty of ± 1.0 events.

To summarize, the number of events expected in this $l^+l^-q\bar{q}$ final state is 27.2 ± 1.7 (syst.), of which 13.0 in the $\mu^+\mu^-q\bar{q}$ final state and 14.2 in the $e^+e^-q\bar{q}$ final state. A total of 29 events is observed, of which 19 $\mu^+\mu^-q\bar{q}$ and 10 $e^+e^-q\bar{q}$ events. One of these events, classified as $e^+e^-q\bar{q}$, is shown in Fig. 12. The agreement still holds when looking at various distributions, e.g. the distributions of the hadronic mass (computed as recoiling against the lepton pair for high masses) or of the leptonic mass, as presented in Fig. 13.

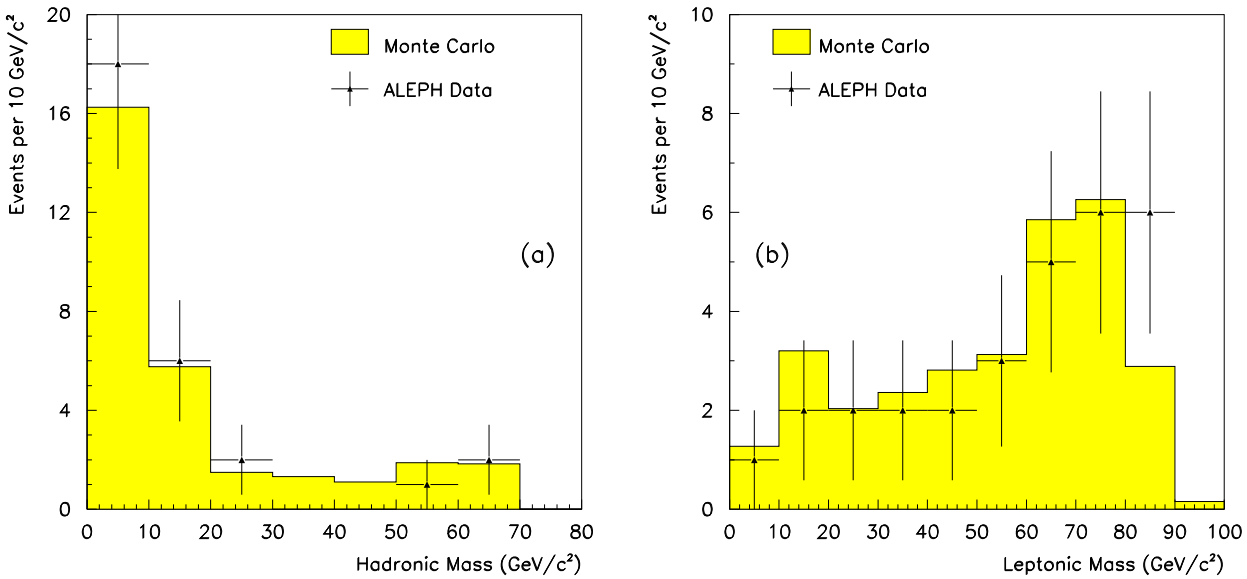

Figure 13: Distributions of the hadronic (a) and the leptonic (b) masses in the $l^+l^-q\bar{q}$ final states, for the data (triangles with error bars) and for the Monte Carlo expectation (shaded histogram) with an absolute normalization.

5 Final states with neutrinos

When the charged lepton pair is replaced by a $\nu\bar{\nu}$ pair, a number of diagrams involving photon exchanges become irrelevant. As a result, the conversion processes $e^+e^- \to \gamma^*\nu\bar{\nu}$, with $\gamma^* \to f\bar{f}$, now provide the dominant contribution, instead of the annihilation processes for all the other four-fermion final states. It is thus expected that the $\nu\bar{\nu}$ pairs should concentrate at large masses, while the $f\bar{f}$ pairs should peak toward low masses and low transverse momenta with respect to the beam axis. The relevant topology to be searched for is therefore that of a monojet. Such a search has been extensively reported in Ref. [21]. It essentially consists of selecting events where one hemisphere is free of any detector activity, with a total momentum transverse to the beam axis in excess of $5\%\sqrt{s}$.

Three events were selected in the ALEPH data, in good agreement with the expec-

tation of 2.6 events from the so-called conversion processes $e^+e^- \to \gamma^*\nu\bar{\nu}$, with $\gamma^* \to f\bar{f}$, while no events were retained in any of the Monte Carlo samples simulating Z decays into a fermion pair or $\gamma\gamma$ processes. The visible masses, transverse momenta and invisible recoil masses of these events are given in Table 8.

Final state	m_{vis} (GeV/c^2)	p_T (GeV/c)	m_{inv} (GeV/c^2)
e^+e^-	3.3	20.3	61
Hadronic	3.2	6.6	80
Hadronic	5.3	18.5	69

Table 8. Characteristics of the three monojet-like events selected in the ALEPH data.

Two events, an acoplanar e^+e^- pair [22] and a hadronic monojet [21], have unexpectedly large masses and transverse momenta. These two events are shown in Fig. 14.

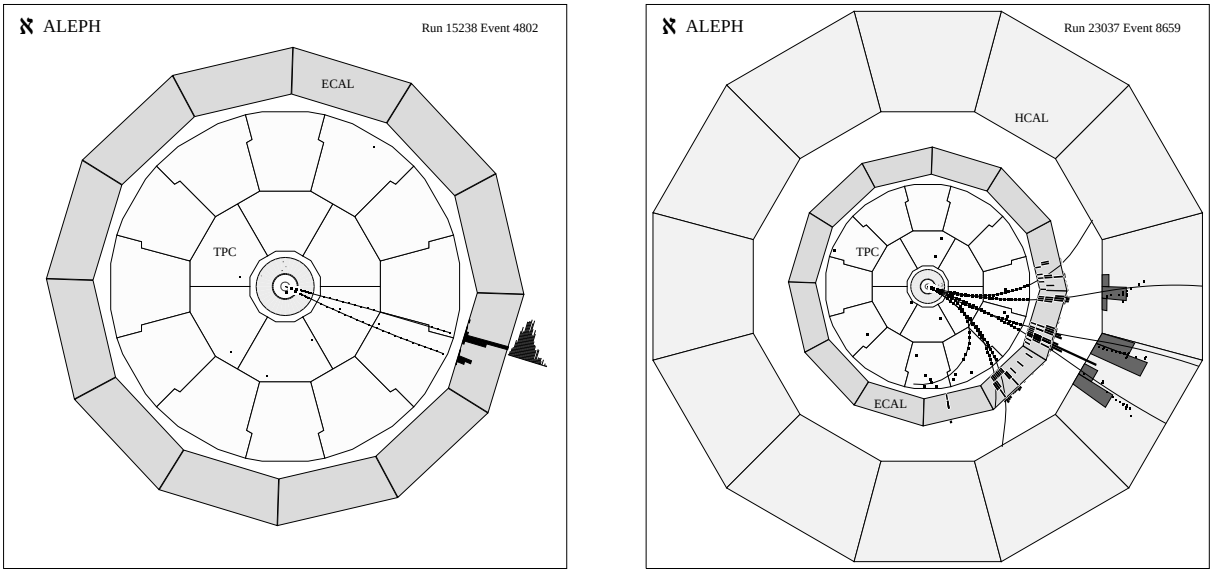

Figure 14: Views of the ALEPH detector for the acoplanar e^+e^- pair and for the hadronic monojet.

It is shown in Ref. [21] that the probability that the three events arise in such a configuration from the conversion diagrams is only 1.0%. When all the processes available in `FERMISV` are taken into account, the number of events expected increases as little as by 0.06, but the probability becomes 2.2%. This indicates that further diagrams not taken into account in `FERMISV` should be considered, namely those involving W exchanges. This has been attempted in Ref. [21], and the result is that a total of 2.75 signal events is expected, with a probability of 4.8% to show up in at least as unlikely a configuration of masses and transverse momenta.

Events with even higher masses, therefore turning into an acoplanar pair of leptons

or of jets in the detector, have been searched for with two analyses developed for the Higgs boson search in the $e^+e^- \to HZ^* \to H\nu\bar{\nu}$ channel, described in Refs. [20] and [22]. No events were found in the ALEPH data, but only 0.25 events are expected from the $e^+e^- \to \nu\bar{\nu}f\bar{f}$ process, and 0.12 events from $e^+e^- \to \tau^+\tau^- f\bar{f}$ where most of the energy of the taus is carried away by the decay neutrinos. A larger integrated luminosity is therefore needed to make a meaningful analysis of this final state at the Z peak.

For both topologies (monojet and acoplanar jets/leptons), the systematic inclusion of all the diagrams pertaining to the four-fermion final state will become necessary to accurately describe the data, and essential as soon as larger centre-of-mass energies will be delivered by LEP. Such programs [23] are presently under development.

6 Conclusion

The large integrated luminosity accumulated by the ALEPH detector at and around the Z peak between 1989 and 1993, equivalent to almost two million hadronic Z decays, has allowed a comprehensive study of the electroweak four-fermion process $e^+e^- \to l\bar{l}f\bar{f}$ to be performed. For all channels studied, the data are found to agree with the standard model of electroweak interactions.

In the four- and six-prong topologies, also called llV topology, arising from the four-lepton final states and also from $l^+l^-q\bar{q}$ at low $q\bar{q}$ masses, 229 events are observed while 235.2 ± 4.7 were expected. The agreement is good in the fifteen groups of llV events, classified according to the three lepton flavours (e, μ and τ) and to the five V types (e^+e^-, $\mu^+\mu^-$, $\pi^+\pi^-$, $\pi^+\pi^-$ or $\mu^+\mu^-$, K^+K^-). In particular, the excess in the $\tau^+\tau^- f\bar{f}$ final state indicated by the ALEPH 1989-1990 data is not confirmed: the 45 events observed agree well with the standard model expectation of 45.5 ± 1.2. Furthermore, the various distributions which were investigated are all consistent with the standard model expectation.

The $l^+l^-q\bar{q}$ final state with larger multiplicity or larger mass $q\bar{q}$ systems was also studied: 29 events are observed, of which 10 $e^+e^-q\bar{q}$ and 19 $\mu^+\mu^-q\bar{q}$. Here again, the number of events and the distributions of characteristic variables are in close agreement with the standard model predictions.

Finally, three monojets events are observed while 2.75 were expected to arise from the $e^+e^- \to \nu\bar{\nu}f\bar{f}$ process. However, the values of their masses and transverse momenta are unlikely at the 5% level. Further study of this channel will require more accurate calculations and more data.

Acknowledgements

We wish to thank our colleagues from the accelerator divisions for the successful operation of LEP. We are indebted to the engineers and technicians in all our institutions for their contribution to the excellent performance of ALEPH. Those of us from non-member countries thank CERN for its hospitality.

References

1. D. Decamp et al., (ALEPH Coll.), *Phys. Lett.* **263B** (1991), 112.
2. T. Azemoon, *"Rare decays of the Z at LEP"*, Proceedings of the XXVI International Conference on High Energy Physics, Dallas, Texas (1992), vol. II, page 1315, Ed. J.R. Sanford.
3. P. Abreu et al., (DELPHI Coll.), *Nucl. Phys.* **B403** (1993), 3;
   A. Adam et al., (L3 Coll.), *Phys. Lett.* **321B** (1994), 283;
   P.D. Acton et al., (OPAL Coll.), *Phys. Lett.* **287B** (1992), 389.
4. The LEP Collaborations ALEPH, DELPHI, L3, OPAL, *"Updated parameters of the Z resonance from combined preliminary data of the LEP experiments"*, CERN-PPE **93-157** (Aug. 1993).
5. D. Decamp et al., (ALEPH Coll.), *Nucl. Instrum. Methods* **A 294** (1990), 121.
6. D. Buskulic et al., (ALEPH Coll.), *"Performance of the ALEPH detector"*, to be submitted to *Nucl. Instrum. and Methods*, in preparation.
7. J.M. Hilgart, R. Kleiss and F. Le Diberder, *Comput. Phys. Commun.* **75** (1993), 191.
8. T. Kinoshita, B. Nižic and Y. Okamoto, *Phys. Rev.* **D31** (1985), 2108.
9. M. Aguilar-Benitez et al., The particle Data Group, *Phys. Rev.* **D50** (1994), 1173.
10. H. Burkhardt, F. Jegerlehner, G. Penso and C. Verzegnassi, *Z. Phys.* **C43** (1989), 497.
11. D. Decamp et al., (ALEPH Coll.), *Phys. Lett.* **264B** (1991), 476.
12. S. Jadach and Z. Was, *Comput. Phys. Commun.* **36** (1985), 191.
13. T. Sjöstrand, *"The Lund Monte Carlo for Jet Fragmentation and e^+e^- physics"*, LU-TP/85-10 (1985).
14. J.E. Campagne and R. Zitoun, *Z. Phys.* **C43** (1989), 469.
15. H. Anlauf et al., CERN-TH/7056-93 (Oct. 1993), submitted to *Comput. Phys. Commun.*

16. M. Böhm, A. Denner and W. Hollik, *Nucl. Phys.* **B304** (1988), 687;
F.A. Berends, R. Kleiss and W. Hollik, *Nucl. Phys.* **B304** (1988), 712.

17. J.A.M. Vermaseren, Contribution to the International Workshop on $\gamma\gamma$ Interactions, Amiens, France (1980), Eds. G.Cochard, and P. Kessler.

18. I.F. Ginzburg and V.G. Serbo, *Phys. Lett.* **109B** (1982), 231.

19. E.A. Kuraev and V.S. Fadin, *Sov. J. Nucl. Phys.* **41** (1995) 466.

20. D. Buskulic et al., (ALEPH Coll.), *Phys. Lett.* **313B** (1993), 299.

21. D. Buskulic et al., (ALEPH Coll.), *Phys. Lett.* **334B** (1994), 244.

22. D. Buskulic et al., (ALEPH Coll.), *Phys. Lett.* **313B** (1993), 312.

23. See for instance: F.A. Berends, R. Kleiss and R. Pittau, *"All electroweak four-fermion processes in e^+e^- collisions"*, INLO-PUB-1/94 and NIKHEF-H/94-09 (April 1994).